BNL-112561-2016-JA

AGU PUBLICATIONS

JGR

Journal of Geophysical Research: Atmospheres

RESEARCH ARTICLE

10.1002/2015JD024543

Key Points:
- Cloud radar Doppler velocities can be used to estimate turbulence even when precipitation is present
- A unified turbulence field can be estimated from below cloud base up to boundary layer cloud tops
- Turbulent and microphysical decomposition of the observed Doppler spectrum width is demonstrated

Correspondence to:
P. Borque,
paloma.borque@mail.mcgill.ca

Citation:
Borque, P., E. Luke, and P. Kollias (2016), On the unified estimation of turbulence eddy dissipation rate using Doppler cloud radars and lidars, *J. Geophys. Res. Atmos.*, *120*, 5972–5989, doi:10.1002/2015JD024543.

Received 20 NOV 2015
Accepted 8 MAY 2016
Accepted article online 12 MAY 2016
Published online 30 MAY 2016

On the unified estimation of turbulence eddy dissipation rate using Doppler cloud radars and lidars

Paloma Borque[1], Edward Luke[2], and Pavlos Kollias[1]

[1]Department of Atmospheric and Oceanic Sciences, McGill University, Montreal, Quebec, Canada, [2]Brookhaven National Laboratory, Upton, New York, USA

Abstract Coincident profiling observations from Doppler lidars and radars are used to estimate the turbulence energy dissipation rate (ε) using three different data sources: (i) Doppler radar velocity (DRV), (ii) Doppler lidar velocity (DLV), and (iii) Doppler radar spectrum width (DRW) measurements. The agreement between the derived ε estimates is examined at the cloud base height of stratiform warm clouds. Collocated ε estimates based on power spectra analysis of DRV and DLV measurements show good agreement (correlation coefficient of 0.86 and 0.78 for both cases analyzed here) during both drizzling and nondrizzling conditions. This suggests that unified (below and above cloud base) time-height estimates of ε in cloud-topped boundary layer conditions can be produced. This also suggests that eddy dissipation rate can be estimated throughout the cloud layer without the constraint that clouds need to be nonprecipitating. Eddy dissipation rate estimates based on DRW measurements compare well with the estimates based on Doppler velocity but their performance deteriorates as precipitation size particles are introduced in the radar volume and broaden the DRW values. Based on this finding, a methodology to estimate the Doppler spectra broadening due to the spread of the drop size distribution is presented. The uncertainties in ε introduced by signal-to-noise conditions, the estimation of the horizontal wind, the selection of the averaging time window, and the presence of precipitation are discussed in detail.

1. Introduction

Turbulence is one of the most important physical processes in the atmospheric boundary layer. Eddies with scales comparable to the boundary layer depth are responsible for the vertical transport of water vapor, momentum, mass, enthalpy, and pollutants, affecting the boundary layer evolution and cloud formation. [e.g., *East and Marshall*, 1954; *Jonas*, 1996; *Xue et al*., 2008; *Wang and Grabowski*, 2009; *Albrecht et al*., 2016]. In cloudy boundary layers, turbulence plays a major role in clouds' lifecycle by strongly influencing their formation, maintenance, and dissipation stages [e.g., *Nicholls and Turton*, 1986; *Bretherton et al*., 2004]. Turbulent motions drive entrainment and mixing in clouds as well as influence cloud microphysics and precipitation formation [*Pruppacher and Klett*, 1978; *Shaw et al*., 1998; *Lehmann et al*., 2009; *Bodenschatz et al*., 2010; *Lu et al*., 2013; *Albrecht et al*., 2016]. An improved understanding of in-cloud turbulence can lead not only to a better understanding of cloud lifecycle and cloud microphysical processes but also to an improved representation of clouds in numerical weather prediction and global climate models [*Boutle and Abel*, 2012].

Turbulent eddy dissipation rate (ε in $m^2\ s^{-3}$) represents the rate at which energy cascades from large to small eddies within the inertial subrange. This energy is eventually converted to thermal internal energy in the viscous subrange [*Kolmogorov*, 1941]. An estimation of ε is of importance in the modeling community since it is involved in the parameterization of eddies' average size (or the mixing length), which is needed to solve the nonlinearity of the turbulence equations [e.g., *Kolmogorov*, 1941; *Stull*, 1988]. Estimations of ε are also a key factor in describing cloud lifecycle since varying levels of enhanced turbulence regions can intensify the collision kernel for cloud droplets [e.g., *Khain et al*., 2015]. Measurements of eddy dissipation rate in clear and cloudy regions of the boundary layer have been conducted for decades. Early measurements of ε were based on in situ techniques [*Kaimal et al*., 1976; *Lemone and Pennell*, 1980; *Nicholls*, 1989]. In the last several years, active remote sensing techniques based on profiling Doppler radars and lidars have been developed [*Bryant and Browning*, 1975; *Kollias and Albrecht*, 2000; *Kollias et al*., 2001; *Shupe et al*., 2012; *O'Connor et al*., 2010; *Röhner and Träumner*, 2013; *Fang et al*., 2014]. In particular, profiling cloud radars [*Kollias et al*., 2007] have sufficient sensitivity to detect boundary layer clouds and the high temporal and spatial resolutions needed to resolve all-important vertical motions within clouds. Similarly, Doppler lidars have sufficient sensitivity to detect aerosol particles and comparably high resolution to measure the vertical motion in the entire boundary layer below the cloud base or in clear-sky conditions [*Lamer and Kollias*, 2015].

Previous studies have demonstrated the potential of the aforementioned active remote sensing retrieval techniques and evaluated their accuracy using independent measurements [e.g., *Shupe et al*., 2012; *O'Connor et al*., 2010]. Here two different retrieval techniques are applied to boundary layer cloud cases. One is based on the frequency analysis of time series as applied to two independent data sets: Doppler radar and Doppler lidar velocity measurements (DRV and DLV, respectively). The second is based on the analysis of the Doppler radar spectrum width measurements (DRW) [*Doviak and Zrnić*, 1993]. All eddy dissipation rate estimates are compared at cloud base. The opportunity for such a comparison stems from the availability of several ground-based sites with collocated Doppler cloud radar and Doppler lidar observations. This can lead to ε estimates in both clear and cloudy parts of the boundary layer. However, careful comparison of different eddy dissipation rates in the overlap areas (where more than one estimate is available) is required before unified (above and below cloud base) estimates can be provided. The collocation of ε estimates provides the opportunity to evaluate several factors that could affect their accuracy (e.g., presence of precipitation size particles in the radar sampling volume). Observations used in this work correspond to data collected at the Atmospheric Radiation Measurement (ARM) Mobile Facility deployed in Cape Cod and at the ARM Southern Great Plains site during precipitating and nonprecipitating cloud conditions at both locations. The most important outcome of this comparison is the analysis of the eddy dissipation rate retrievals in both drizzling and nondrizzling regions. This is very important since it suggests that eddy dissipation rate can be estimated throughout the cloud layer regardless of the size of the hydrometeors present in the radar volume. This allows for the routine retrieval of the ε profile in stratiform clouds without the constraint that clouds need to be nonprecipitating. Furthermore, the analysis of cloud-topped boundary layers in marine and continental environments presents the opportunity to analyze the structure, height, and time variability of turbulence in these very distinct regimes. In addition to eddy dissipation rate retrievals, a radar Doppler spectrum decomposition into its dynamical and microphysical broadening terms is shown. This can lead to improved microphysical retrievals of hydrometeor particle size distributions. Finally, this study offers a comprehensive analysis of the possible factors that can introduce biases and uncertainties into eddy dissipation rate estimates.

2. Eddy Dissipation Rate Retrieval Techniques

Traditionally, measurements of ε were obtained from turbulence sensors mounted on fixed towers or carried on tethered balloons [*Kaimal et al*., 1976; *Caughey et al*., 1979; *Zhou et al*., 1985; *Zhu et al*., 2001] and from aircraft equipped with different gust-wind-probes systems [*Nicholls*, 1978; *Lemone and Pennell*, 1980; *Brost et al*., 1982; *Nucciarone and Young*, 1991]. Remote sensing observations have also been used in the past to generate eddy dissipation rate estimates. Several methods have been proposed for cloudy conditions involving ground radar observations. The most common techniques are based on times series of vertical velocities [e.g., *Bryant and Browning*, 1975; *Kollias and Albrecht*, 2000; *Kollias et al*., 2007; *Shupe et al*., 2012; *Fang et al*., 2014]. Similarly, below cloud base or in clear-sky conditions, Doppler lidar observations can be used to generate turbulence estimates ([e.g., *O'Connor et al*., 2010; *Röhner and Träumner*, 2013; *Tonttila et al*., 2015]—a review of turbulence measurements using ground-based lidars can be found in *Sathe and Mann* [2013]). In particular for cloud and weather radars, measurements of spectrum width can also be used to derive ε, although more restrictive conditions apply to this methodology [e.g., *Doviak and Zrnić*, 1993; *Chapman and Browning*, 2001; *Melnikov and Doviak*, 2009; *Fang et al*., 2014]. A quick review of these remote sensing techniques follows.

2.1. Vertical Velocity Time Series Technique

In the case of homogeneous and isotropic turbulence, the statistical representation of the turbulent energy spectrum $S(k)$ (in $m^3 s^{-2}$) within the inertial subrange is given by

$$S(k) = \alpha \varepsilon^{2/3} k^{-5/3} \tag{1}$$

where α is the Kolmogorov constant (~0.55) and k is the wave number, which can be related to a length scale (L) by $k = 2\pi/L$, and to frequency (f) by $k = f/V_h$ under the assumption of a linear wind field, where V_h is the horizontal wind speed (Figure 1). It follows from equation (1) that

$$\varepsilon_{DV} = \frac{2\pi}{V_h}\left(\frac{2}{3\alpha}\int_{f_{low}}^{f_{high}} S(f)df\right)\left(f_{low}^{-2/3} - f_{high}^{-2/3}\right)^{-3/2} \tag{2}$$

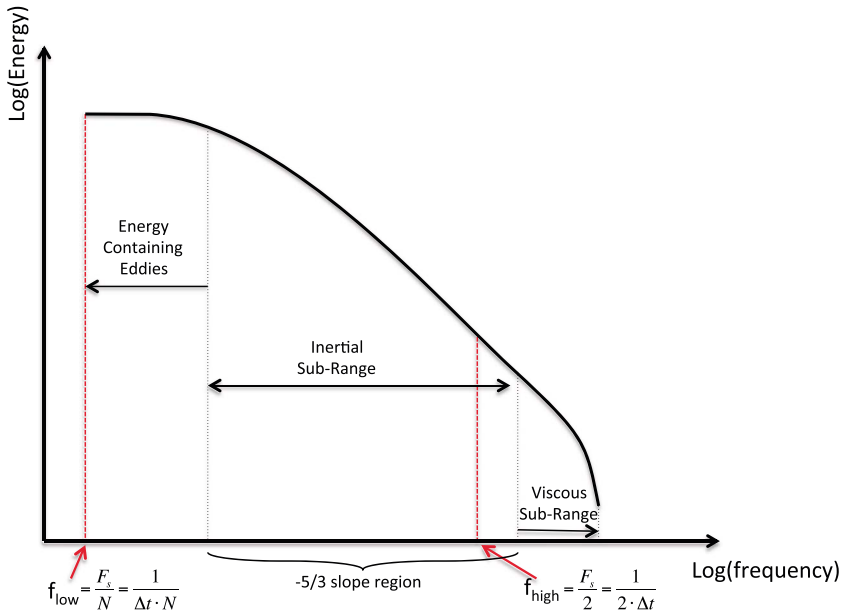

Figure 1. Schematic of turbulence kinetic energy spectrum as a function of frequency. The black dotted lines denote the different regions. The lower and higher frequencies in the spectra are given by the sample size and the time resolution of the instrument (red dotted lines). The red dashed lines represent the highest and lowest frequency with Δt the instrument time resolution and N the sample size. For a sampled time of approximately 25 min (N_{KAZR}: 400 and N_{lidar}: 1220) the lowest frequency $\left(f_{low} = \frac{F_s}{2} = \frac{1}{2\Delta t}\right)$ that can be sampled is ~6.76×10^{-4} s^{-1} and the highest frequency $\left(f_{high} = \frac{F_s}{N} = \frac{1}{N.\Delta t}\right)$ for the KAZR is 0.135 s^{-1} and given the higher temporal resolution of the Doppler lidar this limit is further extended to ~0.41 s^{-1}.

where f_{high} and f_{low} are the limiting frequencies of the inertial subrange. Therefore, fitting this region of the observed spectra to the $k^{-5/3}$ power law yields the ε_{DV} (Figure 1). This estimation of ε heavily relies on the accurate determination of the frequency range of the inertial subrange and the correctness of the $k^{-5/3}$ power law fit. Figure 2 shows an example power spectrum generated from profiling Doppler radar and lidar data at cloud base. Here the inertial subrange is defined by the following three simple steps. First, we compute the slope of the least squares fit for 33 different frequency intervals (Figure 2). Second, all the frequency intervals where the slope of this best linear fit is within 20% of that of the inertial subrange ($-5/3 \pm 1/3$) are classified as having "good fits." Third, ε_{DV} is defined as the mean of all estimates computed for the frequency intervals with good fit according to equation (2). The region of uncertainty of this methodology is defined as the mean ±1 standard deviation of all the estimates with good fit. Note that ε_{DV} bears almost no difference from the median of estimates with good fit or with the estimate computed from the least squares fit with the slope closest to $-5/3$. The uncertainties in the Doppler velocity (DV) technique follow.

2.2. Uncertainties in the Doppler Velocity Technique

The factors that contribute to uncertainty in the estimation of the eddy dissipation rate from the power spectrum of the mean Doppler velocity time series are discussed here. First, we address the methodology used in the selection of the frequency interval over which the power law fitting is performed. If a fixed frequency interval is chosen, it is possible that the inertial range is not correctly selected and the slope criterion is then not satisfied. The search over a wide range of frequencies proposed here yields better results and minimizes the cloud regions where no retrievals are performed. Another measure of the uncertainty is provided by the standard deviation of the eddy dissipation rate estimates from the frequency intervals where the power law fit satisfies the criterion for fitting.

Another source of uncertainty arises from how accurately the horizontal wind magnitude can be determined. As can be seen from equation (2), ε_{DV} is inversely proportional to the horizontal wind speed. If a small bias (ΔV_h) is introduced, then the relative bias in the ε estimate $\left({}^{\varepsilon_1}/_{\varepsilon_o}\right)$ is given by

$$\frac{\varepsilon_1}{\varepsilon_o} = \frac{V_h}{V_h + \mathrm{DV}_h} \tag{3}$$

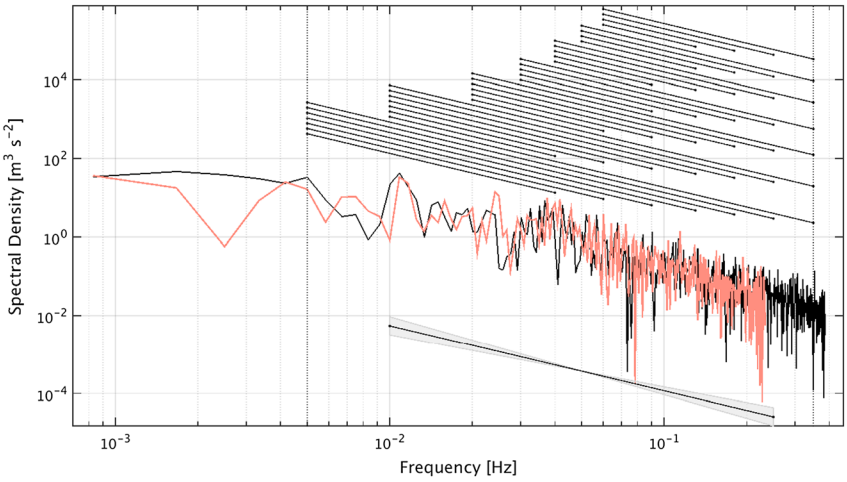

Figure 2. Doppler velocity power spectrum generated for 20 min from data on 15 November 2012 at the PVC site around 15:00 UTC for the vertically pointing cloud radar (red) and the Doppler lidar (black). The black thin lines in the top right corner of the figure represent the different frequency intervals used to retrieve independent eddy dissipation rates, and the grey shaded area in the bottom right corner represents the 20% (slope threshold) departure from the −5/3 slope fit allowed to retrieved ε (solid black line) for the largest frequency interval.

where ε_o and V_h are the true eddy dissipation rate and horizontal wind speed. The dependency of the $\varepsilon_1/\varepsilon_o$ on ΔV_h as a function of the horizontal wind magnitude is shown in Figure 3. The relative bias is smaller for larger horizontal wind speeds and increases considerably for small horizontal wind speeds (Figure 3).

2.3. Doppler Spectrum Width Technique

Estimates of the eddy dissipation rate can be derived from Doppler radar spectrum width measurements. Doppler spectrum width is a measurement of the spread of the radar return signal over the range of radial velocities within the radar sampling volume. Broadening of the spectrum (σ) can occur due to the spread of the hydrometeors' terminal velocity (σ_d), radial (vertical), and transverse (horizontal) wind shear within the scattering volume (σ_s), cross (horizontal) wind within the scattering volume (σ_m), air turbulence (σ_t), antenna rotation (σ_α), and oscillation and/or wobbling of hydrometers (σ_o) [*Doviak and Zrnić*, 1993],

$$\sigma^2 = \sigma_d^2 + \sigma_s^2 + \sigma_m^2 + \sigma_t^2 + \sigma_\alpha^2 + \sigma_o^2 \tag{4}$$

Note that in the case of a vertically pointing cloud radar, the main contributions to σ^2 are reduced to the spread of drop size distribution, wind shear, cross wind, and turbulence resulting in

$$\sigma^2 = \sigma_d^2 + \sigma_s^2 + \sigma_m^2 + \sigma_t^2 \tag{5}$$

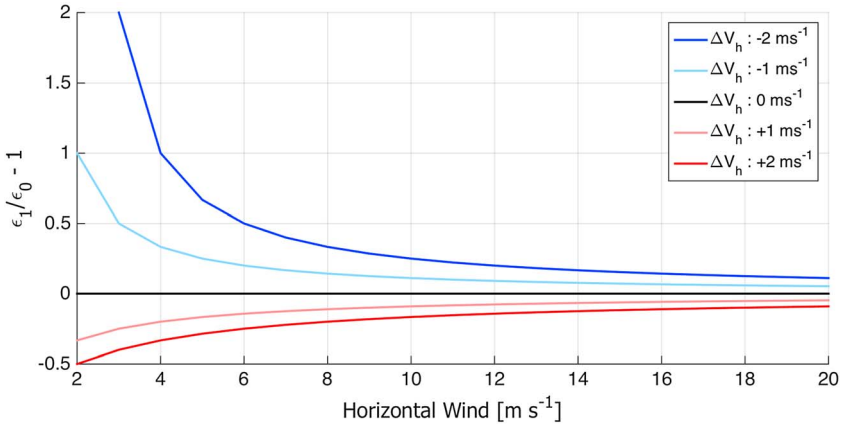

Figure 3. Eddy dissipation rate dependence on horizontal wind speed. Different curves represent the different variations in the horizontal wind speed shown in the upper right plot.

A large spread of hydrometeor sizes leads to a spread in the vertical velocities observed in the radar volume resulting in an increase of the observed spectrum width. In a rain event this contribution is estimated to be around 1 m s^{-1} [*Lhermitte*, 1963]. However, in the presence of cloud droplets alone, σ_d is said to be small and therefore neglected when compared to the influence of the other terms [*Kollias et al*., 2001]. This latter assumption is further analyzed in the next section.

The contribution due to shear of the Doppler velocity in the radar domain (both horizontal and vertical) also causes an increase in the observed spectrum width that can be expressed as [e.g., *Doviak and Zrnić*, 1993]

$$\sigma_s^2 = \sigma_{sx}^2 + \sigma_{sy}^2 + \sigma_{sz}^2 \tag{6}$$

where

$$\sigma_{sx} = \sigma_{sy} = K_x z \sigma_x \tag{7}$$

$$\sigma_{sz} = K_z \sigma_z \tag{8}$$

where K_x and K_z are the wind shear in the directions perpendicular and parallel to the radar beam respectively and z is the height from the radar

$$\sigma_x = \frac{\theta_1}{4\sqrt{ln2}} \tag{9}$$

and

$$\sigma_z = \frac{0.35 c\tau}{2} \tag{10}$$

where θ_1 is the one-way beam width between half-power points, c is the speed of light, and τ is the radar pulse width. For a vertically pointing radar, K_z is estimated by the differences between radial velocities at adjacent heights, and under the assumption of linearity in the horizontal wind field (V_h), K_x is estimated as

$$K_x = \frac{dV_d}{dx} = \frac{1}{V_h}\frac{dV_d}{dt} \tag{11}$$

where V_d is the Doppler velocity.

Finally, the contribution due to horizontal wind within the radar volume can be expressed as

$$\sigma_m = V_h \sigma_x \tag{12}$$

If the broadening due to spread of hydrometeor fall velocities can be neglected (section 2.2), it is possible to estimate the turbulence contribution (σ_t) to the observed spectrum width (σ) from equation (5) once the shear (σ_s) and horizontal wind (σ_m) contributions are removed. Then the turbulent eddy dissipation rate ($\varepsilon_{\mathrm{DRW}}$) can be estimated from σ_t as [e.g., *Labitt*, 1981; *Gossard and Strauch*, 1983; *Doviak and Zrnić*, 1993]

$$\epsilon_{\mathrm{DRW}} \approx \frac{0.72\langle\sigma_t\rangle^3}{z\sigma_x a^{3/2}} \tag{13}$$

for a range resolution smaller than the beam width ($\sigma_z \ll \sigma_x$) and

$$\epsilon_{\mathrm{DRW}} \approx \frac{\langle\sigma_t\rangle^3}{\sigma_z (1.35a)^{3/2}} \left(\frac{11}{15} + \frac{4}{15} z^2 \frac{\sigma_x^2}{\sigma_z^2}\right)^{-3/2} \tag{14}$$

for a beam width smaller than the range resolution ($\sigma_x < \sigma_z$), where σ_t denotes the time average of the turbulence contribution following *Fang et al*. [2014].

Here the uncertainty of this technique is given by the range of possible $\varepsilon_{\mathrm{DRW}}$ values that can be estimated when considering the bias introduced by signal-to-noise ratio in spectrum width. Details of this dependency and additional sources of uncertainties in the DRW technique follows.

2.4. Uncertainties in The Doppler Radar Spectrum Width Technique

A key input to estimating eddy dissipation rate following the DRW technique is the spectral broadening term due to turbulence (σ_t). The estimation of σ_t requires (i) measurement of the total Doppler radar spectrum width based on the discrete Fourier transform (DFT) estimator and (ii) a decision to account for or neglect each of the other factors that can contribute to the observed Doppler spectrum width. The uncertainty

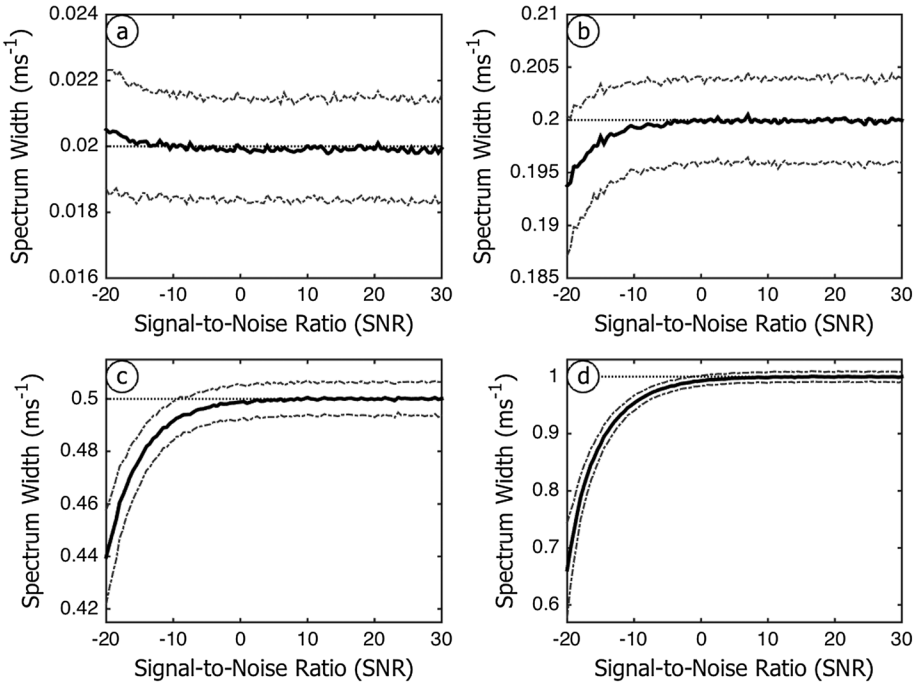

Figure 4. The estimated spectrum width values after 1000 simulations as a function of signal-to-noise ratio for four input spectrum width values (a) 0.02 m s^{-1}, (b) 0.2 m s^{-1}, (c) 0.5 m s^{-1}, and (d) 1.0 m s^{-1}. The velocity resolution of the simulated spectra is 0.0308 m s^{-1}. The black solid line represents the mean spectrum width over 1000 realizations, the black solid thin line the initial spectrum width, and the grey dotted line ±1 standard deviation around the mean value.

introduced in these steps is examined using synthetic Doppler spectra from the McGill Radar Doppler Spectra Simulator [*Kollias et al*., 2005, 2014].

First, the uncertainty and bias introduced by the DFT estimator in low signal-to-noise ratio (SNR) conditions are investigated. One thousand simulations for every set of Doppler spectrum width and SNR values were used. Simulations indicate that at low SNR conditions there is an underestimation of the width of the spectrum [*Doviak and Zrnić*, 1993, *Kollias et al*., 2007] (Figure 4). For narrow spectra (spectrum width smaller than 0.2 m s^{-1}) the effect of low SNR is not as important as for a distribution with wider spectra and it is most important when the spectra have a considerable width, e.g., $\sigma \geq 0.5$ m s^{-1} (Figure 4). Thus, SNR is an important factor to take into account when analyzing spectrum width measurements for eddy dissipation rate retrievals. Radar returns from drizzle-free conditions inherently have low SNR. Similarly, wide radar Doppler spectra at low SNR conditions are not frequently encountered in profiling cloud radars due to their narrow antenna beam width, short pulse length, and integration.

Next, the assumption that the contribution of a cloud particle size distribution via the σ_d term is negligible is evaluated [*Kollias et al*., 2001]. The relative importance of the σ_d term from both cloud and drizzle particle size distributions is evaluated for a wide range of turbulence intensity conditions expressed in terms of eddy dissipation rate. Here a simplified version of equation (4) is used, with the variance of spectrum width only depending on turbulence and drop size distribution, i.e, $\sigma^2 = \sigma_t^2 + \sigma_d^2$. The influence of σ_d^2 is then analyzed with the ratio σ_d^2/σ^2 where values close to one (zero) indicate that the spread of the hydrometeors' size (turbulence) dominates, and a value of 0.5 shows that both terms contribute equally to the variance of the spectrum width. This ratio is analyzed for a case dominated by cloud droplets and for a drizzle case independently. The shape of the cloud and drizzle particle size distributions is assumed to be lognormal [*Miles et al*., 2000] with the parameters shown in Table 1. For reflectivity values below −35 dBZ σ_d^2 is always smaller than σ_t^2 even for a very weakly turbulent environment with $\varepsilon = 10^{-6}$ m^2 s^{-3} (Figure 5a). This ratio is always smaller than 0.2 for all values of ε equal to or larger than 5×10^{-4} m^2 s^{-3} ($\sigma_t \geq 0.25$ m s^{-1}) showing that for these values of turbulence the spread of the drop size distribution accounts only for less than 20% (which represents 28% error in ε) of the total, thus leading to a turbulence dominated spectrum width (Figure 5a). For a less turbulent environment

Table 1. Parameters for the Lognormal Distribution

	Cloud Drops	Drizzle Drops
N (m^{-3})	1×10^9	1×10^6
σ_x	20	10
r_0 (μm)	Varying from 8 to 60 every 1	Varying from 40 to 500 every 10
σ_t ($m\,s^{-1}$)	Varying from 0.05 to 0.6 ever 0.02	Varying from 0.05 to 2 every 0.05

(e.g., $\varepsilon \leq 1 \times 10^{-4}\,m^2\,s^{-3} - \sigma_t \geq 0.15\,m\,s^{-1}$) the same percentage can be reached for reflectivity values lower than −20 dBZ. This shows that the previous assumption that the contribution of the spread of the hydrometeor size does not play a major role in the width of the spectrum is correct. Thus, the spectral broadening due to cloud-only droplets can be neglected. As expected, this is not the case for drizzle particle size distributions. For example, in an environment with low to medium levels of turbulence ($\varepsilon \geq 1 \times 10^{-4}\,m^2\,s^{-3}$) the spread of the drop size distribution is the dominant factor regardless of reflectivity, whereas it was shown that it has a minor effect in a cloud-only scenario (Figure 5).

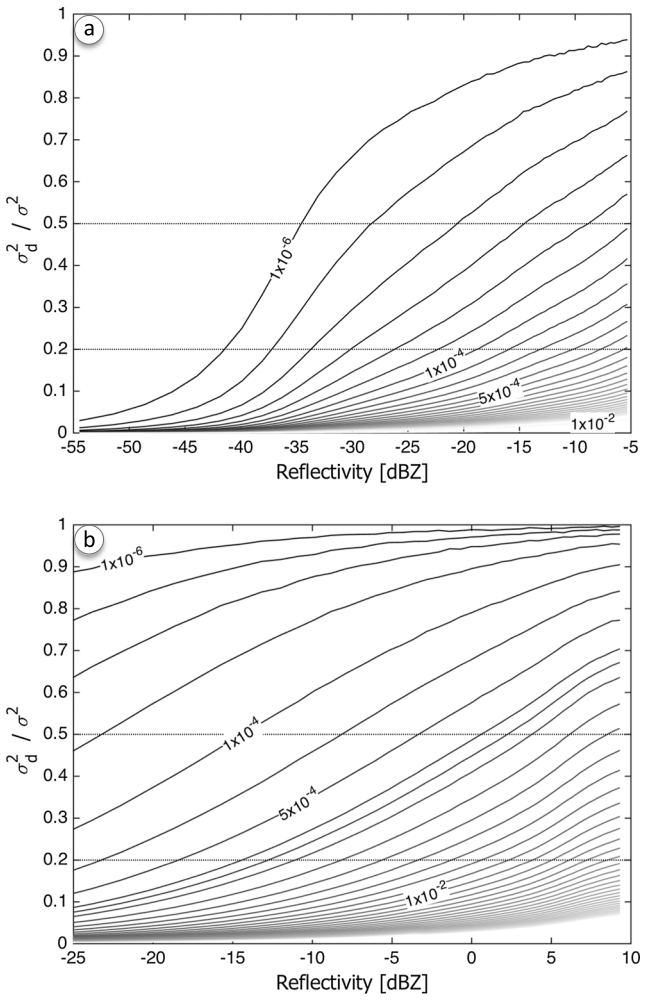

Figure 5. The ratio of the velocity variance due to the drop size distribution to the total simulated spectrum variance $\left(\sigma_d^2/\sigma^2 = \sigma_d^2/\left(\sigma_d^2 + \sigma_t^2\right)\right)$ as a function of reflectivity values for (a) a population of cloud droplets represented by lognormal distribution with $N = 10^9\,m^{-3}$, r_0 ranging from 8 to 60μm (every 2 μm) and $\sigma_x = 0.2$, and for (b) a drizzle population with $N = 10^6\,m^{-3}$, r_0 ranging from 40 to 500 μm (every 10 μm) and $\sigma_x = 0.1$. The contribution of turbulence (σ_t) ranges from 0.05 $m\,s^{-1}$ to 0.6 $m\,s^{-1}$ every 0.02 $m\,s^{-1}$ for the cloud scenario and from 0.05 $m\,s^{-1}$ to 2 $m\,s^{-1}$ every 0.05 $m\,s^{-1}$ for drizzle. The darker colors represent a less turbulent environment. Additional contours of $\varepsilon = 1 \times 10^{-6}\,m^2\,s^{-3} - \sigma_t = 0.7\,m\,s^{-1}$, $\varepsilon = 5 \times 10^{-4}\,m^2\,s^{-3} - \sigma_t = 0.25\,m\,s^{-1}$, $\varepsilon = 1 \times 10^{-4}\,m^2\,s^{-3} - \sigma_t = 0.15\,m\,s^{-1}$, and $\varepsilon = 1 \times 10^{-2}\,m^2\,s^{-3} - \sigma_t = 0.0032\,m\,s^{-1}$ are also shown.

Finally, the influence of the wind shear term in the determination of the observed radar Doppler spectrum is evaluated. The contribution of wind shear to spectrum width can be divided into its two components (vertical and horizontal, σ_{sz}^2 and σ_{sx}^2) and analyzed according to their contributions separately. The σ_{sz}^2 is mainly a function of the variation of Doppler velocity with height (equation (8)), whereas σ_{sx}^2 is a function of the variation of Doppler velocity in time, the horizontal wind, and the height of the radar sampling volume (equations (7) and (11)). Here similarly as for the drop size distribution term, equation (4) is simplified so that only the turbulence and wind shear terms affect the variance of spectrum width (i.e., $\sigma^2 = \sigma_t^2 + \sigma_{sz}^2$ or $\sigma^2 = \sigma_t^2 + \sigma_{sx}^2$ depending on which component is under analysis), and the ratio σ_t^2/σ^2 is used to analyze its relative importance. In a low turbulence regime ($\varepsilon < 1 \times 10^{-5}\,m^2\,s^{-3}$; $\sigma_t < 0.07\,m\,s^{-1}$), vertical shear of Doppler velocity plays a major role in the spectrum width especially for strong shear values (Figure 6). However, in an environment with a medium to high turbulence ($\varepsilon \geq 1 \times 10^{-4}\,m^2\,s^{-3}$), the contribution of vertical shear to spectrum width

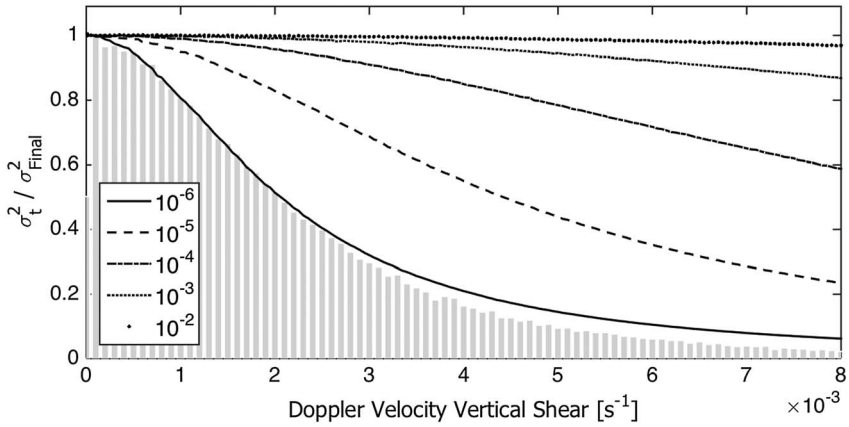

Figure 6. Influence of the vertical variation of Doppler velocity within three range gates of the radar in the shear contribution to total simulated spectrum width for different turbulence scenarios (lines). The influence of the shear term is quantified as the fraction of the turbulence contribution to the variance of the total spectrum width $\left(\sigma_t^2/\sigma^2 = \sigma_t^2/\left(\sigma_s^2+\sigma_t^2\right)\right)$. Values close to zero (one) represent a major contribution from shear (turbulence) to the total spectrum width. Shear is computed for the KAZR range resolution (~30 m). The normalized histogram of observed vertical shear of Doppler velocity for the two cases analyzed is also displayed.

decreases quite considerably until it becomes negligible (Figure 6). This conclusion can also be reached when considering the drop size distribution term instead of turbulence, with the vertical shear component becoming negligible in cases with significant values of σ_d (e.g., drizzle events).

The contribution of the horizontal shear is more challenging to analyze since more parameters affect its magnitude. For an environment with medium to high levels of turbulence ($\varepsilon > 1\times10^{-4}\,m^2\,s^{-3}$) there is little to no contribution from the horizontal shear regardless of the height of the retrieval or the crosswind affecting the system (Figures 7 and 8). Similarly, the horizontal shear term does not tend to play an important role in the width of the spectrum when relatively high crosswinds ($V_h > 2\,m\,s^{-1}$) are present (Figures 7 and 8). The height dependency of the contribution from the horizontal shear influences the width of the spectrum. For low-level clouds, in an environment with very low turbulence (e.g., $\varepsilon \le 1\times10^{-6}\,m^2\,s^{-3}$) and weak crosswinds ($V_h \le 0.5\,m\,s^{-1}$) σ_s^2 can play a major role in the spectrum width for extreme changes in the Doppler velocity with time (Figure 7a). On the other hand, for high-level retrievals the horizontal shear contribution can be as important as σ_t for medium levels of turbulence ($\varepsilon = 1\times10^{-4}\,m^2\,s^{-3}$) and it becomes the dominant factor affecting the width of the spectrum for small values of turbulence (Figure 8a).

Therefore, it is important to consider the influence of the wind shear on the spectrum width for environments with medium to low turbulence and low crosswinds. Under these conditions it can be the dominant factor impacting the width of the spectrum especially when the Doppler velocity is highly changing in time and/or height.

3. Eddy Dissipation Rate Comparison Between Doppler Lidar and Cloud Radar Retrievals

The observations analyzed here were collected at two U.S. Department of Energy (DOE) Atmospheric Radiation Measurement (ARM) program Climate Research Facility (ACRF) sites [*Mather and Voyles*, 2013]. The analysis focuses on two periods with low-level stratiform clouds with and without drizzle for which observations from a profiling cloud radar, a Doppler lidar, and a ceilometer are available. Coincident observations of Doppler radar and lidar enable the estimation of the eddy dissipation rate using all techniques near the cloud base.

3.1. Cape Cod Maritime Stratiform Cloud

The first case analyzed was observed during the ARM Mobile Facility 2012 deployment in Cape Cod, Massachusetts for a 12 month period as part of the Two Column Aerosol Project (TCAP, campaign.arm.gov/tcap/). The instrumentation at the site included a 95 GHz W-band ARM Cloud Radar (WACR), a

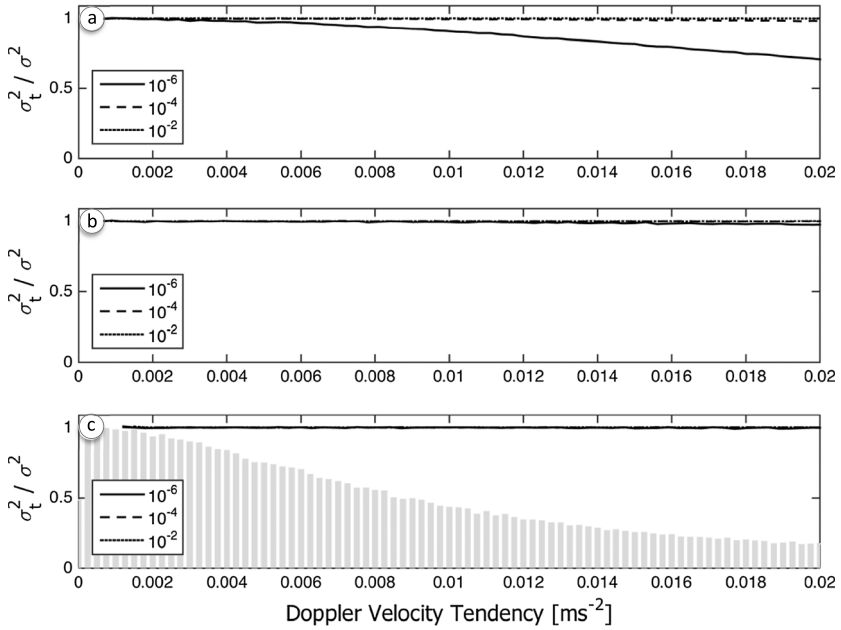

Figure 7. Influence of the temporal variation of Doppler velocity within two consecutive scans in the shear contribution to total simulated spectrum width for a low (ε: 10^{-6} m^2 s^{-3}—solid line), medium (ε: 10^{-4} m^2 s^{-3}—dashed line), and high turbulent scenario (ε: 10^{-2} m^2 s^{-3}—dotted line) for low (a), medium (b), and high (c) horizontal wind conditions. The influence of the shear term is quantified as the fraction of the contribution of turbulence to the variance of the total spectrum width $\left(\sigma_t^2/\sigma^2\right)$. Estimations are made at a height of 500 m. Tendencies are computed for the KAZR time resolution (~3.7 s). The normalized histogram of observed Doppler velocity tendency for the two cases analyzed is also displayed.

Doppler lidar, and a laser ceilometer. The main technical characteristics of the WACR are shown in Table 2. The horizontal wind used for the estimation of the eddy dissipation rates at this site is from interpolated soundings available every 6 h. The selected case was observed on 15 November 2012. A thin cloud layer is present at the beginning of the day with high cloud base (1 km) (Figures 9a and 9b). Throughout the

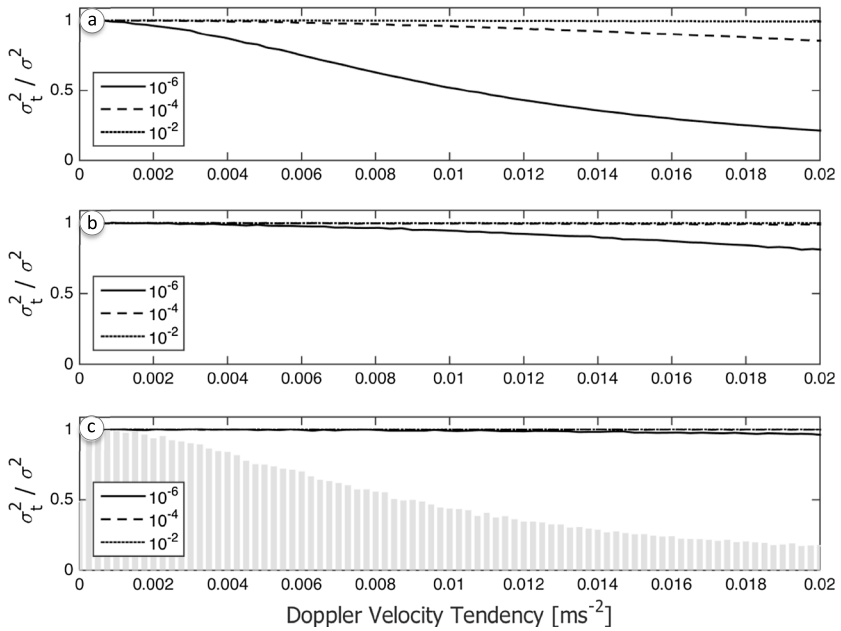

Figure 8. Idem Figure 7 for retrieval height of 1500 m.

Table 2. Technical Specifications of the W-band ARM Cloud Radar on Cape Code Massachusetts and of the Ka-band ARM Zenith Radar Located at the SGP Site

	Radar Properties	
Name	W-Band ARM Cloud Radar (WACR)	Ka-Band ARM Zenith Radar (KAZR)
Location	Cape Code, Massachusetts (PVC)	Lamont, Oklahoma (SGP)
Nyquist velocity (m s^{-1})	7.89	5.96
Range resolution (m)	42.86	30
Time resolution (s)	2.14	3.69
PW (ns)	300	300
Frequency (GHz)	95.04	34.83
Wavelength (mm)	3.15	8.61
Antenna Diameter (m)	1.22	3.05

day the cloud layer deepens with a lowering cloud base (to around 600 m), while the cloud top remains at a constant height throughout the day (~1.3 km). Despite the mismatch in sampling volumes, the mean Doppler velocity time series from the cloud radar and Doppler lidar at the cloud base correlate very well, $r^2 = 0.88$, at the beginning of the period (before 10:00 UTC) (Figure 9c). After 12:00 UTC columns with high

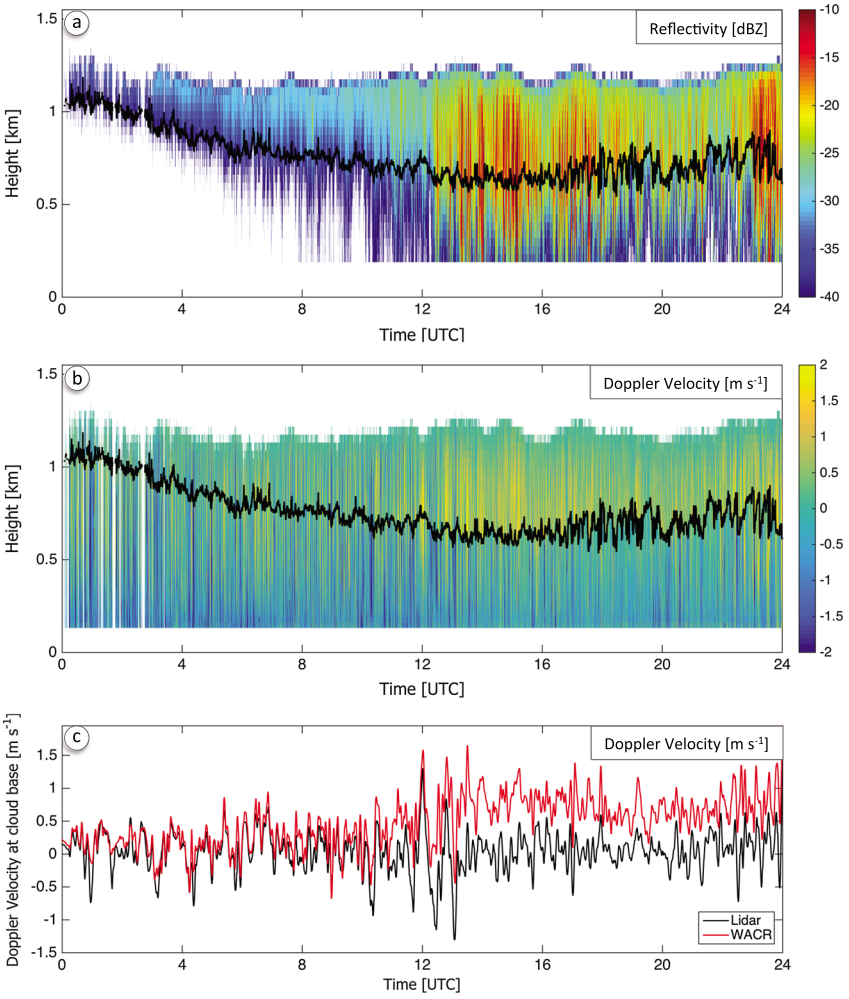

Figure 9. Time-height plot of (a) WACR's reflectivity (a) and of the (b) Doppler velocity from the Doppler lidar and the Doppler radar below and above the cloud base height respectively. Cloud base as detected by the ceilometer is also shown in each panel (black line). (c) Time series of smoothed Doppler velocity from the WACR (black) and the Doppler lidar (red) observed at cloud base. All measurements are for the PVC site on 15 November 2012. Note that positive values represent downward Doppler velocities.

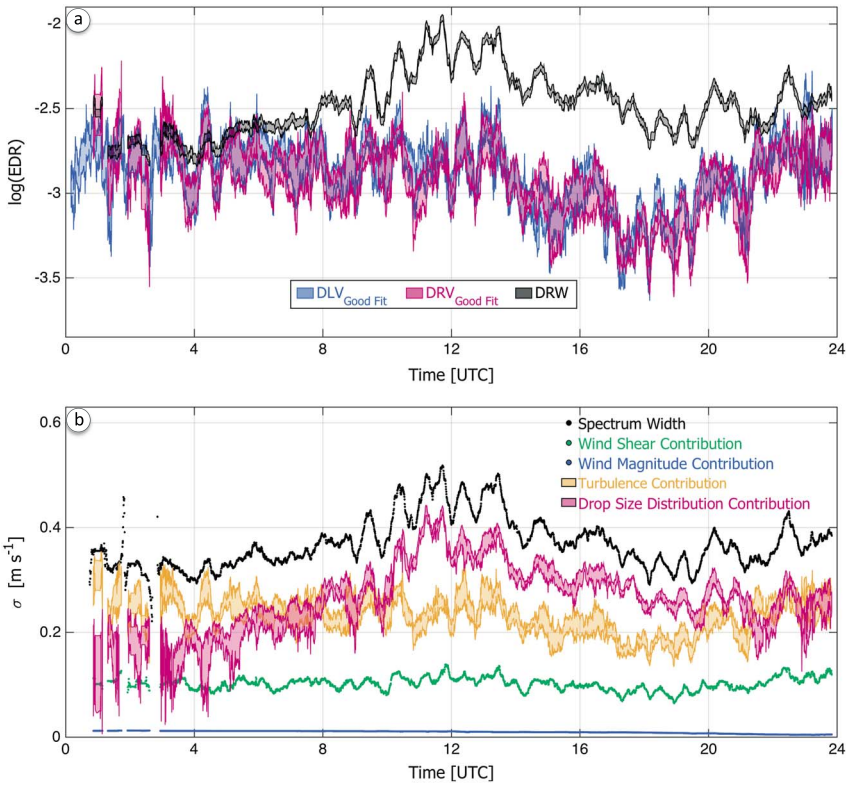

Figure 10. (a) Time series of eddy dissipation rate retrieved from the DRV (purple), the DLV (blue), and the DRW (green) techniques and (b) contributions of wind magnitude (blue), shear contribution (green), turbulence (yellow), and drop size distribution (purple) to spectrum width (black). All measurements and estimates are for the PVC case on 15 November 2012 at cloud based.

values of reflectivity (~ −10 dBZ) associated with higher downward Doppler velocities (positive values) are observed by the WACR (Figures 9a and 9b). At this point the correlation between the vertical velocities observed by the WACR and the Doppler lidar at cloud base height is reduced, $r^2 = 0.78$, and a noticeable offset of 0.5 to 0.75 m s^{-1} is observed (Figure 9c). As expected, the sedimentation velocity of the larger particles dominates the WACR Doppler velocity since the radar backscatter energy is proportional to the sixth moment of the particle diameter. On the other hand, the Doppler lidar is practically unaffected by the larger drizzle particles since its backscatter is proportional to the second moment of the particle diameter [*Luke et al.*, 2010].

3.2. TCAP Results

The temporal evolutions of eddy dissipation rate computed following the methodologies based on Doppler velocity (ε_{DV}) and on Doppler radar spectrum width (ε_{DRW}) are shown in Figure 10a. These retrievals were estimated over a 20 min sampling window (for the WACR's temporal resolution of 2.14 s, this implied a 560-point window, and 985-point window for the Doppler lidar with its 1.22 s time resolution) just above the cloud base (for WACR observations—ε_{DRV} and ε_{DRW}) and just below the cloud base (for lidar observations—ε_{DLV}). The ranges of uncertainty for the different techniques are defined following the definitions presented in section 2.1.

During most of the period analyzed, ε_{DV} estimated at cloud base has very good agreement for both WACR and Doppler lidar measurements (Figure 10a). The retrieved ε_{DV} from these two independent sources not only falls within their region of uncertainty but also has a very similar temporal variability throughout the entire period of analysis (Figure 10a). The correlation coefficient between the mean ε_{DV} estimated from both sensors for this case is 0.86. This indicates that it is possible to determine the eddy dissipation rate from radar Doppler velocities even at times when large particles are present in the radar volume.

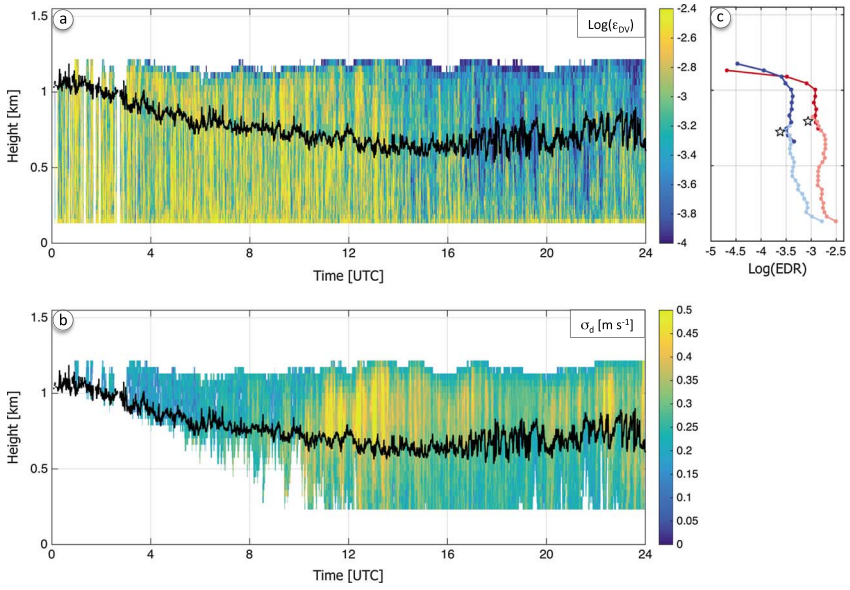

Figure 11. (a) Time-height unified eddy dissipation rate and (b) drop size distribution contribution to spectrum width—σ_d at the PVC site on 15 November 2012. Cloud base as detected by the ceilometer is also shown in each panel (black line). Note that positive values represent downward Doppler velocities. (c) Vertical profile of half an hour average of eddy dissipation rate before precipitation is present below cloud base around 07:00 UTC (warm colors) and afterward, around 19:00 UTC (cold colors). The star denotes the half an hour mean of the height of the cloud base for both periods. Light (dark) colors correspond to Doppler Lidar (radar) retrievals.

Assuming that turbulence is the only factor that contributes to the observed width of the radar Doppler spectrum, turbulent eddy dissipation rates can also be estimated from spectrum width values (ε_{DRW}) based on the methodology presented in section 2.2. These estimates present a reasonably good agreement with those derived using the methodology based on Doppler velocity time series when no precipitating particles are present below the cloud base (i.e., before 08:00 UTC) (Figures 9a and 10a). After 08:00 UTC, ε_{DRW} estimates are higher than ε_{DV}, implying that our initial assumption (i.e., turbulence is the only factor that contributes to the observed Doppler spectrum width) is not valid at this time. Consistent with an absence of precipitating particles, the WACR reflectivity at cloud base is low at the beginning of the period (-40 to -35 dBZ) and gradually increases reaching values slightly above -5 dBZ after 12:00 UTC (Figure 9a). This is indicative of the presence of drizzle drops near the cloud base and shows the clear influence of the drop size distribution term (σ_d) in ε_{DRW} and how neglecting this term in equation (5) leads to an overestimation of turbulence eddy dissipation rates once larger particles are detected in the radar sampling volume. The radar Doppler spectrum width has a more complicated temporal evolution that in general does not correlate well with the WACR reflectivity (figure not shown). This is to be expected since at this radar reflectivity range both microphysics and dynamics contribute to the observed Doppler spectrum width values.

An indication of the spread in the retrieved ε_{DV} value is shown in Figure 10. When the retrieved eddy dissipation rate corresponds to the fit with the logarithmic slope closest to $-5/3$, the median ε_{DV} at cloud base for the entire 24 h period of this case is 5.87×10^{-5} m^2 s^{-3}. However, when ε_{DV} is estimated using the fit with the steepest (more gentle) slope, this leads to a 24 h median of 3.94×10^{-5} m^2 s^{-3} (8.42×10^{-5} m^2 s^{-3}). This difference is not constant throughout the period analyzed but it clearly shows how sensitive this retrieval technique is to the selection of the frequency interval and that an incorrectly chosen inertial subrange can lead to large discrepancies in the retrieved eddy dissipation rate (Figure 11b).

As an example of the uncertainty introduced by the horizontal wind a bias of 1 m s^{-1} was introduced in the calculations. This lead to a 24 h median ε_{DV} of 5.01×10^{-5} m^2 s^{-3}, whereas a bias of -1 m s^{-1} in the horizontal wind lead to a 24 h median of 6.97×10^{-5} m^2 s^{-3}. This bias was selected as it represents an extreme error that can occur for the horizontal wind. However, a larger modification in the horizontal wind (~2 m s^{-1}) introduces an uncertainty in the ε estimate comparable to that introduced by the selection of the frequency interval.

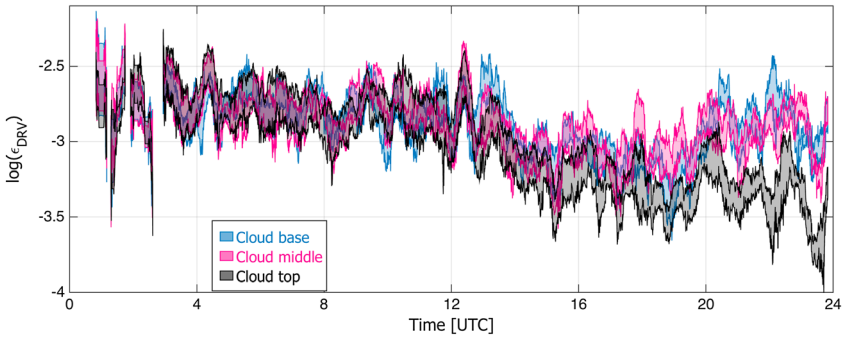

Figure 12. Time evolution of eddy dissipation rate (ε_{DRV}) at the cloud base (blue), middle (purple), and top (black) from the WACR at the PVC site on 15 November 2012.

In the absence of any other information, the decomposition of the microphysical and dynamical contributions to the observed radar Doppler spectrum width is challenging [*Kollias et al.*, 2011]. In this case, however, ε_{DRV} provides the additional source of information necessary to estimate σ_d. Considering ε_{DRV} as a best estimate of the eddy dissipation rate, then the turbulence term (σ_t) can be estimated from equation (14) and the wind shear (σ_s) and the cross wind (σ_m) terms can be estimated from equations (6) and (12), respectively. Once all the different terms affecting the width of the spectrum are computed, the impact of the spread in hydrometeor terminal velocities (σ_d) can be estimated as a residual from equation (5). The contribution of each factor to the observed radar Doppler spectrum width at cloud base is shown in Figure 10b. Turbulence is likely to play a major role at the beginning of the period, when the cloud is likely to be in its development stage and σ_t is the most important term affecting the width of the spectrum (Figures 9a and 10). As the cloud evolves and larger values of reflectivity are detected (from 06:00 to 10:00 UTC), both σ_t and σ_d have similar impacts on spectrum width. Once precipitating particles are detected below cloud base, σ_d becomes the most influential factor in determining the width of the spectrum (Figures 9a and 10). Shear of the Doppler velocity and the magnitude of the horizontal wind have an almost constant influence on spectrum width, with σ_s representing a very small portion of it and σ_m having a minimal impact on the total spectrum width (Figure 10b).

Expanding the aforementioned methodology in height, a continuous field of eddy dissipation rates can be generated at observation sites where collocated Doppler lidar and cloud radar are available. Subsequently, the contribution of the spread in the hydrometeor terminal velocities to spectrum width can also be estimated for a continuous two-dimensional field. The time variability of in-cloud turbulence and the spread of the drop size distribution are similar throughout the different cloud levels, especially at times of no precipitation (Figures 11 and 12). This shows that turbulence plays an important, and very similar, role throughout the entire cloud-to-surface system (Figure 11). The cloud top, however, is less turbulent by the end of the period but it exhibits the same behavior as the base and middle of the cloud (Figure 12). Particularly noteworthy are the consistency and coherency in height of the turbulence patterns estimated by both instruments with the results converging at cloud base (Figures 10 and 11). This is further confirmation that the turbulent eddy dissipation rates estimated by these two independent sensors are likely to be correct.

3.3. Southern Great Plains Continental Stratiform Cloud

The second case analyzed was observed at the ARM Southern Great Plains (SGP) site on 20 November 2011 (Figure 13). The instruments used here include a 35 GHz Ka-band ARM zenith radar (KAZR with a time resolution of 3.69 s), a Doppler lidar (with a temporal resolution of 1.21 s), and a laser ceilometer. The main technical characteristics of the KAZR are shown in Table 2. The evolution of the cloud field during this day was first captured by the KAZR as virga, with hydrometeors present below the cloud base but not reaching the surface (Figure 13a). After 12:00 UTC the cloud reflectivity increased with two main cores (~10 dBZ) covering almost the entire cloud layer with precipitation reaching the surface at around 15:00 UTC. Afterward, it diminished in intensity transitioning into a nonprecipitating shallow stratiform cloud with a thickness of ~250 m (Figure 13a).

The horizontal wind used for the estimation of eddy dissipation rates in this section is from the ARM the Merge-Sounding Value-Added Product. This product presents the thermodynamics of the atmosphere at

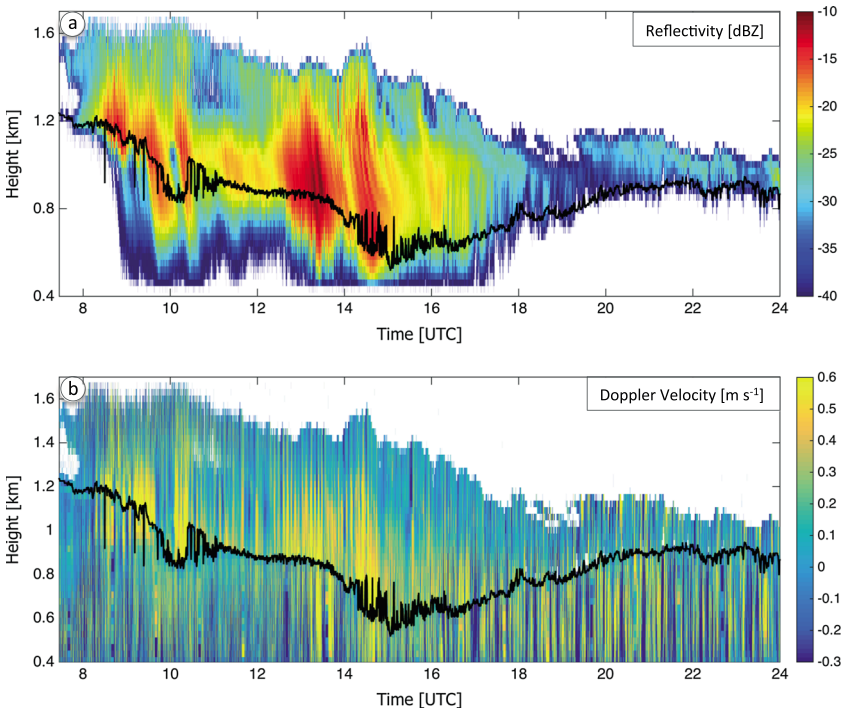

Figure 13. (a) Time-height plot of KAZR's reflectivity and (b) Doppler velocity from the Doppler lidar and KAZR below and above the cloud base height, respectively, on 20 November 2011 at the SGP site. Cloud base as detected by the ceilometer is also shown in each panel (black line). Note that positive values represent downward Doppler velocities.

266 height levels and with 1 min time resolution. It is derived from a combination of surface weather station, radiosonde, and microwave radiometer observations merged with model output from the European Centre for Medium Range Weather Forecasts (further information about this product can be found in *Troyan* [2012]).

3.4. SGP Results

The SGP case exhibits greater cloud top and base height variability, and in terms of radar moments, reflectivity values are similar to those observed at TCAP; however, the observed Doppler velocities and spectrum width values are lower than those at TCAP. The ε_{DRV} and ε_{DLV} estimates show a good agreement in terms of magnitude and variability at the cloud base (Figure 14a); however, the correlation between both estimates for this case (0.78) is smaller than for the TCAP case. When no precipitation size particles are detected below the cloud base by the radar (after 17:00 UTC) these estimates also agree with the spectrum width estimate (ε_{DRW}) as well (Figures 14a). At the beginning of the period (08:00–17:00 UTC) the radar detects precipitation size particles and the broadening term of the drop size distribution dominates the width of the spectrum (Figure 14b). Turbulence and shear contributions play a minimal role at this time but as soon as the cloud weakens (lower reflectivity values) with no echo present below cloud base (after 17:00 UTC) turbulence increases its importance and at times becomes the most dominant term in determining the observed spectrum width (around 18:30 UTC). Similar to the TCAP case, the effect of the crosswind term is at least an order of magnitude smaller than the other factors contributing to the broadening of the spectrum width (Figure 14b).

The two-dimensional dynamical structure of the SGP case is also more complex than the TCAP case (Figure 15). In-cloud air is much less turbulent ($\sim 1 \times 10^{-7}\,m^2\,s^{-3}$) in this event, whereas the subcloud environment is significantly more turbulent ($\sim 1 \times 10^{-3}\,m^2\,s^{-3}$) (Figure 15a). Low-turbulence regions located at cloud base early in the period, around 10:00 UTC, extend upward and reach cloud top after 16:00 UTC (Figure 15a). Cloud-top turbulence is maximum at nighttime, around 09:00 UTC (03:00 local time) and then decreases until 17:00 UTC (11:00 local time) (Figures 15a and 16). The maximum cloud top turbulence occurs as expected at times when net radiative cooling is the strongest and the daytime decrease in turbulence is consistent with the longwave cooling being partially compensated by radiative shortwave warming. Differently, cloud base

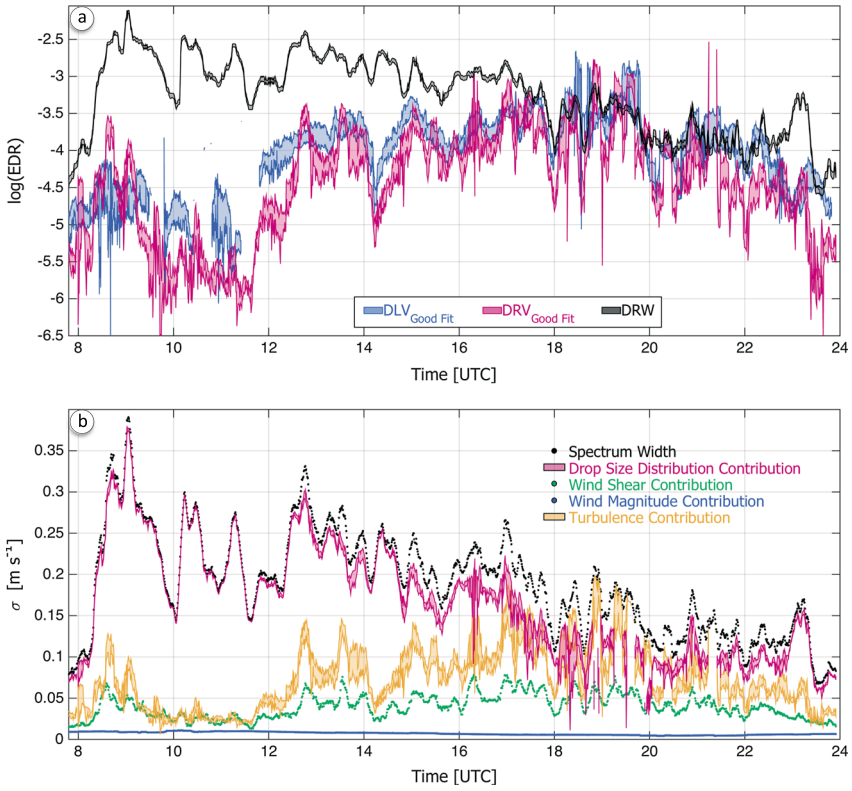

Figure 14. (a) Time series of eddy dissipation rate retrieved from the DRV (purple), the DLV (blue), and the DRW (green) techniques and (b) contributions of wind magnitude (blue), shear contribution (green), turbulence (yellow), and drop size distribution (purple) to spectrum width (black). All measurements and estimates are for the SGP case on 20 November 2011 at cloud based.

turbulence increases after 12:00 UTC and reaches its peak around 19:00 UTC (Figure 16). This increase in turbulence at time of maximum insolation is in clear agreement with the coupling of cloud base and the subcloud layer dynamics. It is also interesting to note that high values of turbulence occur when precipitation is present below cloud base, from 12:00 to 14:00 UTC (Figures 13 and 16). This suggests that evaporation

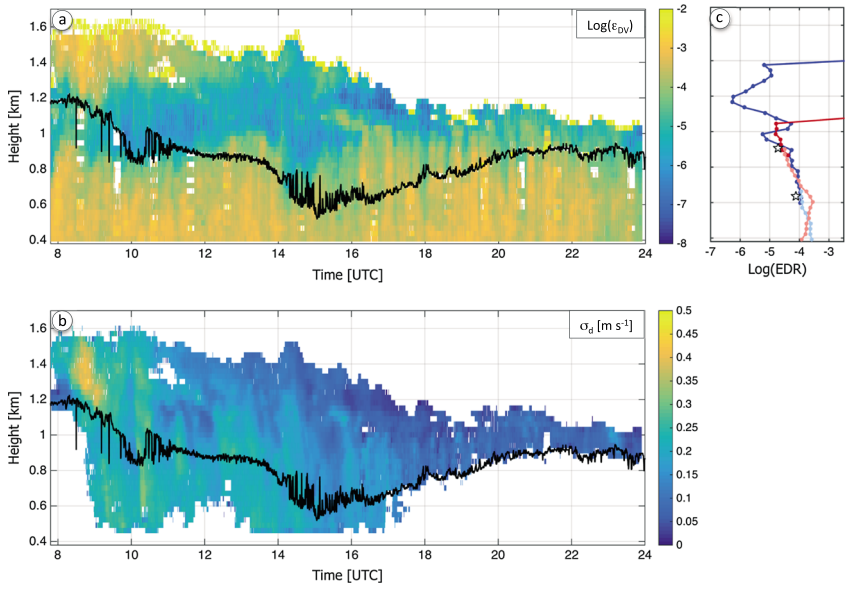

Figure 15. Idem Figure 11 but for the SGP site on 20 November 2011 and the time average performed for 07:00 UTC and 19:00 UTC.

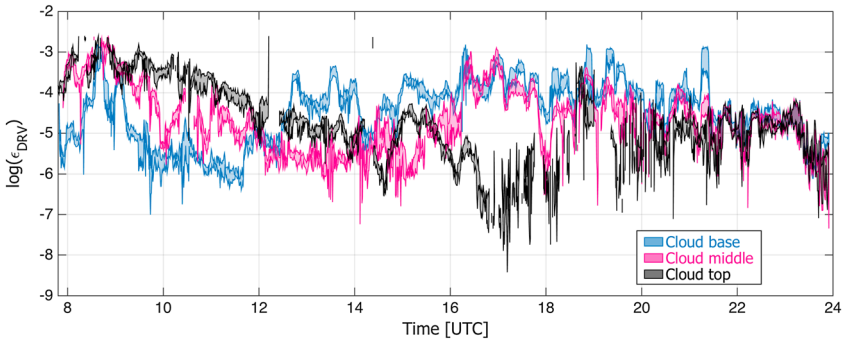

Figure 16. Idem Figure 12 but for the SGP site on 20 November 2011.

cooling could also be playing a major role in the generation of turbulence near cloud base at this time [e.g., *Zhu et al.*, 2010; *Kudo*, 2013]. Turbulence at midcloud is likely to be coupled to the most turbulent region of the cloud as it follows the same behavior as cloud top at nighttime (08:00 to 14:00 UTC) to then be linked to cloud base dynamics at daytime (from 16:00 UTC onward) (Figure 16).

4. Summary

A comprehensive analysis and comparison of two techniques to estimate turbulent eddy dissipation rates from profiling millimeter Doppler radars and Doppler lidars near the cloud base of warm stratiform clouds with and without precipitation were presented. The main objectives of this study are to (i) compare the ε estimates based on time series of mean Doppler velocity measurements from radars and lidars, (ii) compare the ε estimates from the time series-based method with the method based on radar Doppler spectrum width measurements, and (iii) generate a decomposition of the turbulent and microphysical contributions to the observed Doppler spectrum width.

Estimates of ε can be derived from time series of mean Doppler velocity measurements. This technique is based on the estimation of the vertical velocity power spectrum and can generate turbulence estimates below cloud base or in clear-sky conditions (using Doppler lidar observations), and above cloud base (for cloud radar measurements). This estimation of turbulent eddy dissipation rates heavily depends on (i) the objective determination of the inertial subrange frequency limits and (ii) a fitting of this region of the observed spectrum to a $-5/3$ power law in order to retrieve the ε. In the methodology described here, ε estimates are computed for all the frequency intervals where the slope of the fit is within 20% of $-5/3$. The pool of ε estimates is used to derive the mean and a range of uncertainty. On average, for the two cases presented here, the uncertainty estimated using this approach is about 30%. Another source of uncertainty in this methodology arises from the determination of the horizontal wind, which shows a clear impact in increasing the total uncertainty, especially for low horizontal wind speeds.

Estimates of ε are also derived from the Doppler radar spectrum width measurements. This methodology is only applicable within the cloud layer, and below it as well where precipitation is present. For profiling cloud radars, broadening of the Doppler spectrum can occur due to the spread of drop terminal velocities, radial and transverse wind shear within the scattering volume, cross wind within the scattering volume, and air turbulence. It is shown that the contribution of the spread of the hydrometeors' sizes (i.e., fall velocities) can be neglected in drizzle-free conditions. Under this constraint, ε can be estimated from the observed Doppler spectrum width once the shear and horizontal wind contributions are removed.

These ε retrievals were applied to two distinct events of low-level shallow stratiform clouds with and without drizzle collected at the DOE ARM program ACRF sites. The first case was observed on 15 November 2012 during the ARM Mobile Facility deployment in Cape Cod (TCAP), and the second case was observed at the ARM SGP site on 20 November 2011. Observations at both sites included measurements from a profiling Doppler radar, a Doppler lidar and a ceilometer.

In both cases, the temporal evolution and magnitude of the retrieved ε estimated using the vertical velocity measurements from profiling Doppler cloud radar and Doppler lidar at cloud base are in very good agreement for the entire period analyzed. This demonstrates that it is possible to use Doppler radar velocities

to estimate eddy dissipation rate even when larger particles are present in the radar volume. Thus, a unified (below and above the cloud base height using two different sensors) turbulence retrieval is possible, and examples were presented here.

Furthermore, ε retrievals from spectrum width values are in good agreement with those derived using the methodology based on Doppler velocity time series when no precipitating particles are present in the radar volume. Therefore, when all the assumptions for the different methodologies are fulfilled (i.e., when the contributions from Doppler velocity shear and turbulence are the main factors affecting the width of the spectrum and when the inertial subrange is correctly determined) all estimates converge to the same eddy dissipation rate value.

An important implication of the conditional agreement of the two techniques at the cloud base height is that we can attempt a decomposition of the turbulent and microphysical contributions to the observed radar Doppler spectrum width (Figures 11 and 15). This makes it possible to generate fields of the influence of drop size distribution on the width of the radar Doppler spectrum. This derived σ_d term can be used to constrain retrievals of drizzle properties and hopefully provides a means of comparison for the model community to validate their microphysics parameterizations.

For both cases analyzed here it was shown that turbulence is the most important effect impacting the width of the spectrum when the cloud is likely to be in its development stage. Once precipitating particles are detected below cloud base, the spread of the drop size distribution becomes the most influential factor determining the width of the observed Doppler spectrum with turbulence decreasing its importance considerably. The shear of the Doppler velocity and the magnitude of the horizontal wind have a minimal influence on spectrum width. Overall, the horizontal wind is not likely to impact the width of the spectrum and its effect can be neglected without introducing a larger bias into the results. Therefore, it was shown that for the small radar volumes observed by a cloud radar (0.2°–0.3° radar beam width) microphysics and turbulence are likely to be the dominant factors affecting the width of the observed Doppler spectrum.

This manuscript also presented an analysis of the possible bias introduced by low signal-to-noise ratio (SNR) into the spectrum width values. It was shown that data with low SNR result in an underestimation of the width of the Doppler spectrum. For narrow spectra this effect is not very important but it does have a considerable effect for spectrum width values larger than 0.5 m s^{-1}. Therefore, it is recommended to favor data with high signal-to-noise ratio to avoid a systematic bias toward low values of spectrum width that would lead to a negative bias in the estimate eddy dissipation rates.

Acknowledgments
The authors thank three anonymous reviewers for their helpful suggestions on a previous version of the manuscript. This research was supported in part under Contract DE-SC00112704 by the Atmospheric System Research program of the Office of Biological and Environmental Research of the U.S. Department of Energy. Data used here were obtained from the ARM data archive at http://www.archive.arm.gov

References

Albrecht B. A., M. Fang, and V. P. Ghate (2016), Exploring stratocumulus cloud-top entrainment processes and parameterizations by using Doppler cloud radar observations, *J. Atmos. Sci.*, doi:10.1175/JAS-D-15-0147.1, in press.

Bodenschatz, E., S. P. Malinowski, R. A. Shaw, and F. Stratmann (2010), Can we understand clouds without turbulence?, *Science*, *327*(5968), 970–971.

Boutle, I. A., and S. J. Abel (2012), Microphysical controls on the stratocumulus topped boundary-layer structure during VOCALS-Rex, *Atmos. Chem. Phys.*, *12*, 2849–2863.

Bretherton, C. S., T. Uttal, C. W. Fairall, S. E. Yuter, R. A. Weller, D. Baumgardner, K. Comstock, R. Wood, and G. B. Raga (2004), The EPIC 2001 Stratocumulus Study, *Bull. Am. Meteorol. Soc.*, *85*, 967–977.

Brost, R. A., J. C. Wyngaard, and D. H. Lenschow (1982), Marine stratocumulus layers. Part II: Turbulence budgets, *J. Atmos. Sci.*, *39*, 818–836, doi:10.1175/1520-0469(1982)039<0818:MSLPIT>2.0.CO;2.

Bryant, G. W., and K. A. Browning (1975), Multi-level measurements of turbulence over the sea during the passage of a frontal zone, *Q. J. R. Meteorol. Soc.*, *101*, 35–54, doi:10.1002/qj.49710142705.

Caughey, S. J., J. C. Wyngaard, and J. C. Kaimal (1979), Turbulence in the evolving stable boundary layer, *J. Atmos. Sci.*, *36*, 1041–1052.

Chapman, D., and K. A. Browning (2001), Measurements of dissipation rate in frontal zones, *Q. J. R. Meteorol. Soc.*, *127*, 1939–1959.

Doviak, R. J., and D. S. Zrnić (1993), *Doppler Radar and Weather Observations*, 2nd ed., pp. 116–118, Academic Press, San Diego, Calif.

East, T. W. R., and J. S. Marshall (1954), Turbulence in clouds as a factor in precipitation, *Q. J. R. Meteorol. Soc.*, *80*, 26–47.

Fang, M., B. A. Albrecht, V. P. Ghate, and P. Kollias (2014), Turbulence in continental stratocumulus, Part I: External forcings and turbulence structures, *Boundary-Layer Meteorol.*, *150*, 341–360.

Gossard, E. E., and R. G. Strauch (1983), *Radar Observation of Clear Air and Clouds*, pp. 255–258, Elsevier, Amsterdam.

Jonas, P. R. (1996), Turbulence and cloud microphysics, *Atmos. Res.*, *40*, 283–306.

Kaimal, J. C., J. C. Wyngaard, D. A. Haugen, O. R. Coté, Y. Izumi, S. J. Caughey, and C. J. Readings (1976), Turbulence structure in the convective boundary layer, *J. Atmos. Sci.*, *33*, 2152–2169, doi:10.1175/1520-0469(1976)033<2152:TSITCB>2.0.CO;2.

Khain, A. P., et al. (2015), Representation of microphysical processes in cloud-resolving models: Spectral (bin) microphysics versus bulk parameterization, *Rev. Geophys.*, *53*, 247–322, doi:10.1002/2014RG000468.

Kollias, P., and B. Albrecht (2000), The turbulence structure in a continental stratocumulus cloud from millimeter-wavelength radar observations, *J. Atmos. Sci.*, *57*, 2417–2434, doi:10.1175/1520-0469(2000)057<2417:TTSIAC>2.0.CO;2.

Kollias, P., B. A. Albrecht, R. Lhermitte, and A. Savtchenk (2001), Radar observations of updrafts, downdrafts, and turbulence in fair-weather cumuli, *J. Atmos. Sci.*, *58*, 1750–1766.

Kollias, P., B. Albrecht, E. E. Clothiaux, M. A. Miller, K. L. Johnson, and K. P. Moran (2005), The Atmospheric Radiation Measurement Program Cloud Profiling Radars: An evaluation of signal processing and sampling strategies, *J. Atmos. Oceanic Technol.*, *22*, 930–948.

Kollias, P., M. A. Miller, E. P. Luke, K. L. Johnson, E. E. Clothiaux, K. P. Moran, K. B. Widener, and B. A. Albrecht (2007), The Atmospheric Radiation Measurement Program cloud profiling radars: Second-generation sampling strategies, processing, and cloud data products, *J. Atmos. Oceanic Technol.*, *24*, 1199–1214.

Kollias, P., J. Remillard, E. Luke, and W. Szyrmer (2011), Cloud radar Doppler spectra in drizzling stratiform clouds: 1. Forward modeling and remote sensing applications, *J. Geophys. Res.*, *116*, D13201, doi:10.1029/2010JD015237.

Kollias, P., S. Tanelli, A. Battaglia, and A. Tatarevic (2014), Evaluation of EarthCARE cloud profiling radar Doppler velocity measurements in particle sedimentation regimes, *J. Atmos. Oceanic Technol.*, *31*, 366–386.

Kolmogorov, A. N. (1941), Dissipation of energy in locally isotropic turbulence, *Dokl. Akad. Nauk SSSR*, *32*, 16–18.

Kudo, A. (2013), The generation of turbulence below midlevel cloud bases: The effect of cooling due to sublimation of snow, *J. Appl. Meteorol. Climatol.*, *52*, 819–833, doi:10.1175/JAMC-D-12-0232.1.

Labitt, M. (1981), Coordinated radar and aircraft observations of turbulence. Project Rep. ATC 108, Lincoln Lab., MIT, 40 pp.

Lamer, K., and P. Kollias (2015), Observations of fair-weather cumuli over land: dynamical factors controlling cloud size and cover, *Geophys. Res. Lett.*, *42*, 8693–8701, doi:10.1002/2015GL064534.

Lehmann, K., H. Siebert, and R. A. Shaw (2009), Homogeneous and inhomo-geneous mixing in cumulus clouds: Dependence on local turbulence structure, *J. Atmos. Sci.*, *66*, 3641–3659, doi:10.1175/2009JAS3012.1.

Lemone, M. A., and W. T. Pennell (1980), A comparison of turbulence measurements from aircraft, *J. Appl. Meteorol.*, *19*, 1420–1437, doi:10.1175/1520-0450(1980)019<1420ACOTMF>2.0.CO;2.

Lhermitte, R. M. (1963), Motions of scatterers and the variance of the mean intensity of weather radar signals. Rep. SRRC-RR-63-57, Sperry Rand Res. Center, 43 pp.

Lu, C., Y. Liu, S. Niu, S. K. Krueger, and T. Wagner (2013), Exploring parameterization for turbulent entrainment-mixing processes in clouds, *J. Geophys. Res. Atmos.*, *118*, 185–194, doi:10.1029/2012JD018464.

Luke, E. P., P. Kollias, and M. D. Shupe (2010), Detection of supercooled liquid in mixed-phase clouds using radar Doppler spectra, *J. Geophys. Res.*, *115*, D19201, doi:10.1029/2009JD012884.

Mather, J. H., and J. W. Voyles (2013), The ARM Climate Research Facility: A review of structure and capabilities, *Bull. Am. Meteorol. Soc.*, *94*, 377–392, doi:10.1175/BAMS-D-11-00218.1.

Melnikov, V. M., and R. J. Doviak (2009), Turbulence and wind shear in layers of large Doppler spectrum width in stratiform precipitation, *J. Atmos. Oceanic Technol.*, *26*, 430–443, doi:10.1175/2008JTECHA1108.1.

Miles, N. L., J. Verlinde, and E. E. Clothiaux (2000), Cloud droplet size distributions in low-level stratiform clouds, *J. Atmos. Sci.*, *57*, 295–311, doi:10.1175/1520-0469(2000)057<0295:CDSDIL>2.0.CO;2.

Nicholls, S. (1978), Measurements of turbulence by an instrumented aircraft in a convective boundary layer over the sea, *Q. J. R. Meteorol. Soc.*, *104*, 653–676.

Nicholls, S. (1989), The structure of radiatively driven convection in stratocumulus, *Q. J. R. Meteorol. Soc.*, *112*, 431–460.

Nicholls, S., and J. D. Turton (1986), An observational study of the structure of stratiform cloud sheets: Part 2. Entrainment, *Q. J. R. Meteorol. Soc.*, *112*, 461–480.

Nucciarone, J. J., and G. S. Young (1991), Aircraft measurements of turbulence spectra in the marine stratocumulus-topped boundary layer, *J. Atmos. Sci.*, *48*, 2382–2392, doi:10.1175/1520-0469(1991)048<2382:AMOTSI>2.0.CO;2.

O'Connor, E. J., A. J. Illingworth, I. M. Brooks, C. D. Westbrook, R. J. Hogan, F. Davies, and B. J. Brooks (2010), A method for estimating the turbulent kinetic energy dissipation rate from a vertically pointing doppler lidar, and independent evaluation from balloon-borne in situ measurements, *J. Atmos. Oceanic Technol.*, *27*, 1652–1664, doi:10.1175/2010JTECHA1455.1.

Pruppacher, H. R., and J. D. Klett (1978), *Microphysics of Clouds and Precipitation*, 714 pp., Reidel, Boston, Mass.

Röhner, L., and K. Träumner (2013), Aspects of convective boundary layer turbulence measured by a dual-doppler lidar system, *J. Atmos. Oceanic Technol.*, *30*, 2132–2142, doi:10.1175/JTECH-D-12-00193.1.

Sathe, A., and J. Mann (2013), A review of turbulence measurements using ground-based wind lidars, *Atmos. Meas. Tech.*, *6*, 3147–3167, doi:10.5194/amt-6-3147-2013.

Shaw, R. A., W. C. Reade, L. R. Collins, and J. Verlinde (1998), Preferential concentration of clouds droplets by turbulence: Effects on early evolution of cumulus cloud droplet spectra, *J. Atmos. Sci.*, *55*, 1965–1976.

Shupe, M. D., I. M. Brooks, and G. Canut (2012), Evaluation of turbulent dissipation rate retrievals from Doppler cloud radar, *Atmos. Meas. Tech. Discuss.*, *5*, 1375–1385, doi:10.5194/amt-5-1375-2012.

Stull, R. B. (1988), *An Introduction to Boundary Layer Meteorology*, chap. 6, 670 pp., Springer, ISBN 978-90-277-2769-5; ISBN 978-90-277-2768-8.

Tonttila, J., E. J. O'Connor, A. Hellsten, A. Hirsikko, C. O'Dowd, H. Järvinen, and P. Räisänen (2015), Turbulent structure and scaling of the inertial subrange in a stratocumulus-topped boundary layer observed by a Doppler lidar, *Atmos. Chem. Phys.*, *15*, 5873–5885, doi:10.5194/acp-15-5873-2015.

Troyan, D. (2012), Merged sounding value-added product technical report. U.S. Department of Energy. DOE/SC-ARM-TR-087. [Available at http://www.arm.gov/publications/tech_reports/doe-sc-arm-tr-087.pdf.]

Wang, L.-P., and W. W. Grabowski (2009), The role of air turbulence in warm rain initiation, *Atmos. Sci. Lett.*, *10*, 1–8.

Xue, H., G. Feingold, and B. Stevens (2008), Aerosol effects on clouds, precipitation, and the organization of shallow cumulus convection, *J. Atmos. Sci.*, *65*, 392–406, doi:10.1175/2007jas2428.1.

Zhou, M. Y., D. H. Lenschow, B. B. Stankov, J. C. Kaimal, and J. E. Gaynor (1985), Wave and turbulence structure in a shallow baroclinic convective boundary layer and overlying inversion, *J. Atmos. Sci.*, *42*, 47–57, doi:10.1175/1520-0469(1985)042<0047:WATSIA>2.0.CO;2.

Zhu, P., B. Albrecht, and J. Gottschalck (2001), Formation and development of nocturnal boundary layer clouds over the Southern Great Plains, *J. Atmos. Sci.*, *58*, 1409–1426, doi:10.1175/1520-0469(2001)058<1409:FADONB>2.0.CO;2.

Zhu, P., B. A. Albrecht, V. P. Ghate, and Z. Zhu (2010), Multiple scale simulations of stratocumulus clouds, *J. Geophys. Res.*, *115*, D23201, doi:10.1029/2010JD014400.